
GARNET: Reduced-Rank Topology Learning for Robust and Scalable Graph Neural Networks

Chenhui Deng¹ Xiuyu Li¹ Zhuo Feng² Zhiru Zhang¹

Abstract

Graph neural networks (GNNs) have been increasingly deployed in various applications that involve learning on non-Euclidean data. However, recent studies show that GNNs are vulnerable to graph adversarial attacks. Although there are several defense methods to improve GNN robustness by eliminating adversarial components, they may also impair the underlying clean graph structure that contributes to GNN training. In addition, few of those defense models can scale to large graphs due to their high computational complexity and memory usage. In this paper, we propose GARNET, a scalable spectral method to boost the adversarial robustness of GNN models. GARNET first leverages weighted spectral embedding to construct a base graph, which is not only resistant to adversarial attacks but also contains critical (clean) graph structure for GNN training. Next, GARNET further refines the base graph by pruning additional uncritical edges based on probabilistic graphical model. GARNET has been evaluated on various datasets, including a large graph with millions of nodes. Our extensive experiment results show that GARNET achieves adversarial accuracy improvement and runtime speedup over state-of-the-art GNN (defense) models by up to 13.27% and 14.7 \times , respectively.

1. Introduction

Recent years have witnessed a surge of interest in graph neural networks (GNNs), which incorporate both graph structure and node/edge attributes to produce low-dimensional embedding vectors that maximally preserve graph structural information (Hamilton, 2020). GNNs have achieved promising results in various real-world applications, such

as recommendation systems (Ying et al., 2018), self-driving car (Casas et al., 2020), protein structure predictions (Senior et al., 2020), and chip placements (Mirhoseini et al., 2021). However, recent studies have shown that adversarial attacks on graph structure accomplished by inserting, deleting, or rewiring edges in an unnoticeable way, can easily fool the GNN models and drastically degrade their accuracy in downstream tasks (e.g., node classification) (Zügner et al., 2018; Zügner & Günnemann, 2019).

In literature, one of the most effective ways to defend GNNs is to purify the graph by removing adversarial graph structures. Entezari et al. (2020) first observe that graph adversarial attacks mainly affect high-rank properties of the graph; consequently, a low-rank graph should be first constructed by performing truncated singular value decomposition (TSVD) on the graph adjacency matrix, which can then be exploited for training a robust GNN model. Later, Jin et al. (2020) propose Pro-GNN to jointly learn a new graph and its robust GNN model with the low-rank constraints imposed by the graph structure. Although prior low-rank approximation methods largely eliminate adversarial components in graph spectrum, they involve dense adjacency matrices during the GNN training stage, which will lead to much higher time and space complexity, prohibiting their applications in large-scale graph learning tasks.

In addition, due to the high computational cost of TSVD, existing low-rank based methods can only preserve top r singular components (e.g., $r = 50$). Consequently, as shown in Figure 1(a), prior low-rank based methods may lose a wide range of clean graph spectrum that corresponds to important structures of the clean graph in the spatial domain. This is confirmed in Figure 1(c), where the clean accuracy of the TSVD-based method largely increases when preserving more spectral information via increasing the graph rank r . In other words, prior low-rank approximation methods eliminate high-rank adversarial components at the cost of inevitably impairing the important (clean) graph structure, which degrades the overall quality of the reconstructed graph and therefore limits the performance of GNN training.

In this work, we propose GARNET, a novel spectral approach to learning the underlying clean graph topology of an adversarial graph via combining spectral embedding with

¹Cornell University, New York, USA. ²Stevens Institute of Technology, New Jersey, USA.. Correspondence to: Chenhui Deng <cd574@cornell.edu>, Zhuo Feng <zhuo.feng@stevens.edu>, Zhiru Zhang <zhiruz@cornell.edu>.

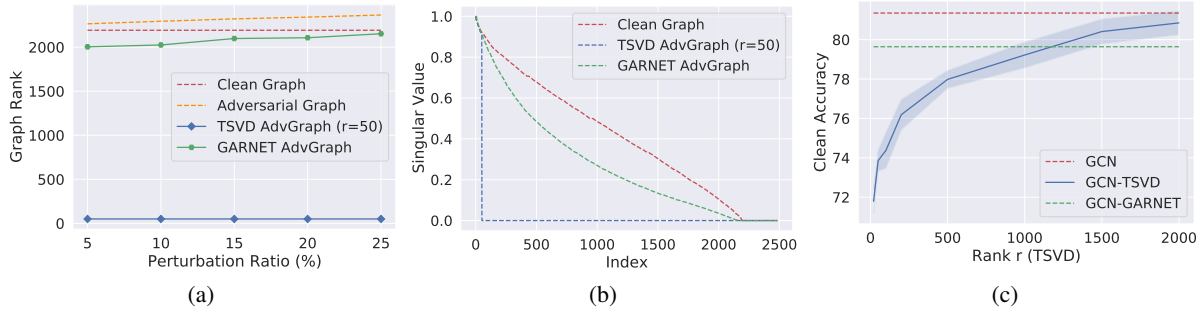


Figure 1. “TSVD AdvGraph” and “GARNET AdvGraph” denote adversarial graphs purified by TSVD and GARNET, respectively. (a) Graph rank comparison on Cora under Metattack with different perturbation ratio. (b) Singular value comparison of different normalized graph adjacency matrices on Cora. (c) Accuracy \pm std. of GCN-TSVD on Cora with different r -rank approximation via TSVD.

probabilistic graphical model (PGM), where the learned graph structure encodes the conditional dependence among low-dimensional node representations (spectral embedding vectors) (Dong et al., 2019). More concretely, given an adversarial graph, GARNET first constructs a base graph topology by leveraging weighted spectral embeddings that are resistant to adversarial attacks, which is followed by an effective and efficient graph refinement scheme for pruning noncritical edges in the base graph by exploiting PGM.

By recovering the clean graph structure, Figures 1(a) and 1(b) show that the adversarial graph purified by GARNET largely restores the rank of the underlying clean graph. Thus, GARNET can be viewed as a reduced-rank topology learning approach that slightly reduces the rank of the input adversarial graph, which is fundamentally different from the prior low-rank based defense methods (e.g., TSVD and ProGNN). Moreover, GARNET scales comfortably to large graphs due to its nearly-linear algorithm complexity, and produces a sparse yet high-quality graph that improves GNN robustness without involving any dense adjacency matrices during GNN training. As a byproduct, unlike existing defense methods (e.g., ProGNN) that assume graphs to be homophilic, i.e., adjacent nodes in a graph tend to have similar attributes (Zhu et al., 2020), GARNET does not have such an assumption and thus can protect GNNs against adversarial attacks on both homophilic and heterophilic graphs.

We evaluate GARNET on both homophilic and heterophilic datasets under strong graph adversarial attacks such as Nettack (Zügner et al., 2018) and Metattack (Zügner & Günnemann, 2019) with various perturbation settings. Moreover, we further show the nearly-linear scalability of our approach on the ogbn-products dataset that consists of millions of nodes (Hu et al., 2020). Our experimental results indicate that GARNET largely improves both clean and adversarial accuracy over baselines in most cases. Our main technical contributions are summarized as follows:

- To our knowledge, we are the first to exploit spectral graph embedding and probabilistic graphical model for improving robustness of GNN models, which is achieved by learning a

reduced-rank graph topology for recovering the underlying clean graph structure from the input adversarial graph.

- By recovering the critical edges that contribute to maximum likelihood estimation in PGM while ignoring adversarial components, GARNET produces a high-quality graph on which existing GNN models can be trained to achieve high accuracy. Our experimental results show that GARNET gains up to 13.27% adversarial accuracy improvement over state-of-the-art defense baselines.

- Our proposed reduced-rank topology learning method has a nearly-linear complexity in time/space and produces a sparse graph structure for scalable GNN training. This allows GARNET to run up to 14.7 \times faster than prior defense methods on popular data sets such as Cora and Squirrel. In addition, GARNET scales comfortably to very large graph data sets with millions of nodes, while prior defense methods run out of memory even on a graph with 20k nodes.

2. Background

2.1. Undirected Probabilistic Graphical Models

Consider an n -dimensional random vector x that follows a multivariate Gaussian distribution $x \sim N(0, \Sigma)$ with probability density:

$$f(x) = \frac{\exp\left(-\frac{1}{2}x^\top \Sigma^{-1}x\right)}{(2\pi)^{n/2} \det(\Sigma)^{(1/2)}} \propto \det(\Theta)^{1/2} \exp\left(-\frac{1}{2}x^\top \Theta x\right),$$

where $\Sigma = \mathbb{E}[xx^\top] \succ 0$ represents the covariance matrix, and $\Theta = \Sigma^{-1}$ represents the precision matrix (inverse covariance matrix). Given a data matrix $X \in R^{n \times d}$ that includes d i.i.d (independent and identically distributed) samples $X = [x_1, \dots, x_d]$, where $X \sim N(0, \Sigma)$ has an n -dimensional Gaussian distribution with zero mean, the goal of probabilistic graphical models (PGM) is to learn a precision matrix Θ that corresponds to an undirected graph structure \mathcal{G} for encoding the conditional dependence between variables of the observations on columns of X (Banerjee et al., 2008; Friedman et al., 2008). Specifically, the classical graphical Lasso method aims at estimating a sparse Θ through maximum likelihood estimation (MLE) of $f(x)$

leveraging convex optimization (Friedman et al., 2008).

In this work, we focus on one increasingly popular type of Gaussian graphical models, which is also known as attractive Gaussian Markov random fields (GMRFs). Attractive GMRFs restrict the precision matrix to be a Laplacian-like matrix $\Theta = L + \frac{I}{\sigma^2}$, where $L = D - A$ denotes the set of valid graph Laplacian matrices with D and A representing the diagonal degree matrix and adjacency matrix of the underlying undirected graph, respectively, I denotes the identity matrix, and σ^2 is a constant denoting prior data variance. Similar to the graphical Lasso method (Friedman et al., 2008), recent methods for estimating attractive GMRFs leverage emerging graph signal processing (GSP) techniques to solve the following convex problem (Dong et al., 2016; Egilmez et al., 2017; Dong et al., 2019; Kalofolias & Perraudin, 2019; Feng, 2021):

$$\max_{\Theta} \log \det \Theta - \frac{1}{d} \text{tr}(XX^T \Theta) - \alpha \|\Theta\|_1 \quad (1)$$

where $\det(\cdot)$ and $\text{tr}(\cdot)$ denote the determinant and trace operators, respectively, α is a hyperparameter to control the regularization term. The first two terms together can be interpreted as log-likelihood under a GMRF. The last ℓ_1 regularization term is to enforce Θ (and the corresponding graph) to be sparse. If X is non-Gaussian, formulation in (1) can be regarded as Laplacian estimation based on minimizing the Bregman divergence between positive definite matrices induced by the function $\Theta \mapsto -\log \det(\Theta)$ (Slawski & Hein, 2015).

2.2. Graph Adversarial Attacks

Most existing graph adversarial attacks aim at degrading the accuracy of GNN models by inserting/deleting edges in an unnoticeable way (e.g., maintaining node degree distribution) (Sun et al., 2018). The most popular graph adversarial attacks fall into the following two categories: (1) targeted attack, (2) untargeted attack. The targeted attacks attempt to mislead a GNN model to produce a wrong prediction on a target sample (e.g., node), while the untargeted attacks strive to degrade the overall accuracy of a GNN model for the whole graph data set. Dai et al. (2018) first formulate the targeted attack as a combinatorial optimization problem and leverages reinforcement learning to insert/delete edges such that the target node is misclassified. Zügner et al. (2018) propose another targeted attack called Nettack, which produces an adversarial graph by maximizing the training loss of GNNs. Zügner & Günnemann (2019) further introduce Metattack, an untargeted attack that treats the graph as a hyperparameter and uses meta-gradients to perturb the graph structure. It is worth noting that graph adversarial attacks have two different settings: poison (perturb a graph prior to GNN training) and evasion (perturb a graph after GNN training). As shown by Zhu et al. (2021), the poison setting is typically more challenging to defend, as it changes the graph structure that fools GNN training. Thus, in this work,

we evaluate our model against both targeted and untargeted attacks under the poison setting.

2.3. Graph Adversarial Defenses

To defend GNN against adversarial attacks, Entezari et al. (2020) first observe that Nettack, a strong targeted attack, only changes the high-rank information of the adjacency matrix. Thus, they propose to construct a low-rank graph by performing truncated SVD to undermine the effects of adversarial attacks. Later, Jin et al. (2020) propose Pro-GNN that adopts a similar idea yet jointly learns the low-rank graph and GNN model. Although those low-rank approximation based methods achieve state-of-the-art results on several datasets, they produce dense adjacency matrices that correspond to complete graphs, which would limit their applications for large graphs. Moreover, they only preserve a small region of the graph spectrum and thus may lose too much important information corresponding to the clean graph structure in the spatial domain, which limits the performance of GNN training. In addition, most existing defense methods explicitly (or implicitly) assume the underlying graph to be homophilic, which results in rather poor performance when defending GNN models on heterophilic graphs. In contrast to the prior arts, GARNET achieves highly robust yet scalable performance on both homophilic and heterophilic graphs under adversarial attacks by leveraging a novel graph purification scheme based on spectral embedding and graphical model.

3. The GARNET Approach

Recently, Entezari et al. (2020) and Jin et al. (2020) have shown that the well-known graph adversarial attacks (e.g., Nettack and Metattack) are essentially high-rank attacks, which increase graph rank by enlarging the smallest singular values of adjacency matrix when perturbing the graph structure, while rest of the graph spectrum remains almost the same. Consequently, a natural way for improving GNN robustness is to purify an adversarial graph by eliminating the high-rank components of its spectrum.

Low-rank topology learning (prior work). Given an adversarial adjacency matrix $A_{adv} \in R^{n \times n}$, Entezari et al. (2020) propose to reconstruct a low-rank approximated adjacency matrix via performing TSVD: $\hat{A} = U\Sigma V^T$, where $\Sigma \in R^{r \times r}$ is a diagonal matrix consisting of r largest singular values of A_{adv} . $U \in R^{n \times r}$ and $V \in R^{n \times r}$ contain the corresponding left and right singular vectors, respectively. As the largest singular values are hardly affected by graph adversarial attacks, the reconstructed low-rank adjacency matrix \hat{A} is resistant to adversarial attacks.

However, due to the high computational cost of TSVD, \hat{A} is typically computed by only using top r largest singular values and their corresponding singular vectors, where r is a relatively small number (e.g., $r = 50$). Consequently, the rank of \hat{A} is only $r = 50$, which is two orders of magnitude

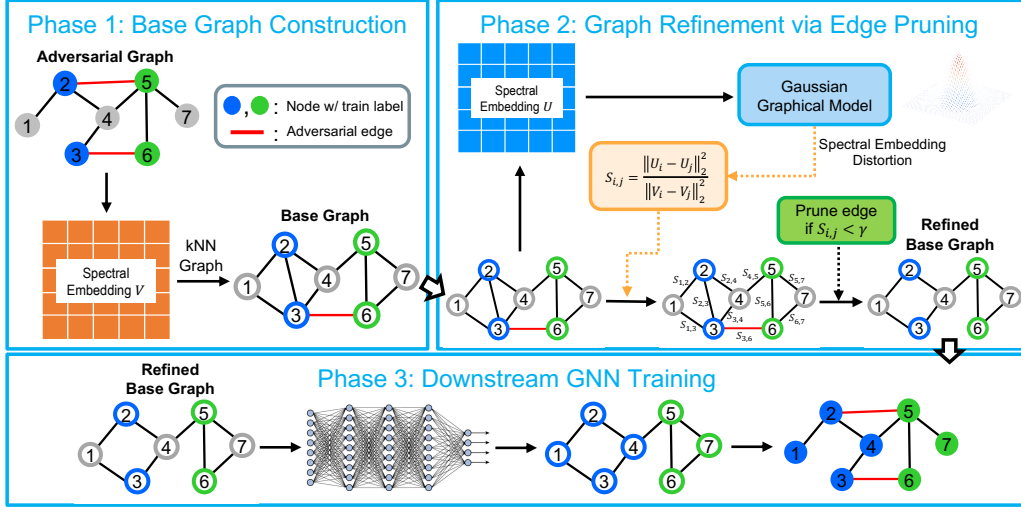


Figure 2. An overview of the three major phases of GARNET.

smaller than the rank of the clean graph, as shown in Figure 1(a). Since these low-rank methods are overly aggressive in reducing the graph rank, \hat{A} may lose too much important spectral information corresponding to the clean graph structure. As shown in Figure 1(c), the clean accuracy of the TSVD-based method is largely improved by increasing the graph rank r , which indicates the low-rank graph obtained with a small r loses the key graph structure contributing to GNN training. Note that the adversarial and clean graphs share most of the graph structure, as adversarial attacks perturb the clean graph in an unnoticeable way. Consequently, losing those important clean graph structures will also limit the performance of GNN on the adversarial graph.

Reduced-rank topology learning (this work). Given the adversarial graph \mathcal{G}_{adv} and its adjacency matrix A_{adv} , our goal is to learn a reduced-rank graph, which slightly reduces the rank of \mathcal{G}_{adv} to mitigate the effects of adversarial attacks, while retaining most of the important graph spectrum corresponding to the clean graph structure. As adversarial attacks mainly affect the least dominant singular components of A_{adv} (Entezari et al., 2020), one straightforward way for constructing such a reduced-rank graph is to utilize all the singular components except those least dominant ones via TSVD. Nonetheless, computing such a large number of singular components is computationally expensive even with efficient numerical solvers (Baglama & Reichel, 2005), and is thus not scalable to large graphs.

To learn the reduced-rank graph in a scalable way, in this work, we leverage only the top few (e.g., 50) dominant singular components of A_{adv} to restore its important graph spectrum, via recovering the corresponding clean graph structure with the aid of PGM. Figure 2 gives an overview of our proposed approach, GARNET, which consists of three major phases. The first phase constructs a base graph by ex-

plotting spectral embedding and a scalable nearest-neighbor graph algorithm. The second phase further refines the base graph by pruning noncritical edges based on PGM. The last phase trains existing GNN models on the refined base graph to improve their robustness. Next, we will first describe our notion of clean graph recovery via PGM as well as the scalability issue of prior PGM-based work in Section 3.1, which motivates us to develop scalable kernels of GARNET, as described in Sections 3.2 and 3.3, respectively. We further provide the overall complexity of GARNET in Section 3.4.

3.1. Graph Recovery via Graphical Model

A general philosophy behind PGM is that there exists an underlying graph G , whose structure determines the joint probability distribution of the observations on the data entities, i.e., columns of a data matrix $X \in R^{n \times d}$, where n is the number of data points, d the dimension per data point. To recover the underlying graph structure from the data matrix X , one common way is to leverage MLE by solving Equation 1 in Section 2.1. As the top few dominant singular components of the adjacency matrix capture the corresponding graph structure, we can naturally construct the data matrix X based on those dominant singular components, and then adopt PGM to recover an underlying graph via MLE. To this end, we define a weighted spectral embedding matrix as follows:

Definition 3.1. Given the top r smallest eigenvalues $\lambda_1, \lambda_2, \dots, \lambda_r$ and their corresponding eigenvectors v_1, v_2, \dots, v_r of normalized graph Laplacian matrix $L_{norm} = I - D^{-\frac{1}{2}}AD^{-\frac{1}{2}}$, where I and A are the identity matrix and graph adjacency matrix, respectively, and D is a diagonal matrix of node degrees, the **weighted spectral embedding matrix** is defined as:

$$V \stackrel{\text{def}}{=} \left[\sqrt{|1 - \lambda_1|}v_1, \dots, \sqrt{|1 - \lambda_r|}v_r \right], \quad (2)$$

whose i -th row $V_{i,:}$ is the **weighted spectral embedding** of the corresponding i -th node in the graph.

Theorem 3.2. *Given a normalized graph adjacency matrix $A_{norm} = D^{-\frac{1}{2}}AD^{-\frac{1}{2}}$ and weighted spectral embedding matrix V of an undirected graph, let \hat{A} be the rank- r approximation of A_{norm} via TSVD. If the top r dominant eigenvalues of A_{norm} are non-negative, then we have $\hat{A} = VV^T$.*

Our proof for Theorem 3.2 is available in Appendix A. Theorem 3.2 shows the connection between weighted spectral embedding and the low-rank adjacency matrix \hat{A} obtained by TSVD. Specifically, the weighted spectral embedding matrix V can be viewed as an eigensubspace matrix consisting of a few dominant singular components of the corresponding adjacency matrix. Thus, we can use V to recover the underlying clean graph via PGM. However, obtaining V requires the knowledge of the clean graph structure, which seems to create a chicken and egg problem.

Fortunately, since the dominant singular components are hardly affected by adversarial attacks (Entezari et al., 2020), the weighted spectral embedding is therefore also resistant to adversarial attacks, indicating that the underlying clean graph \mathcal{G}_{clean} and its corresponding adversarial graph \mathcal{G}_{adv} share almost the same weighted spectral embeddings. As a result, we can exploit the weighted spectral embedding matrix V of \mathcal{G}_{adv} to represent that of \mathcal{G}_{clean} . By replacing the data matrix X with V in Equation 1, we have the following objective function:

$$\max_{\Theta} : F = \log \det \Theta - \frac{1}{r} \text{tr}(VV^T\Theta) - \alpha \|\Theta\|_1 \quad (3)$$

By finding the optimizer Θ^* in Equation 3, we can recover the underlying graph that maximizes the likelihood given the observation on the weighted spectral embedding matrix V . However, solving Equation 3 requires at least $O(n^2)$ time/space complexity for each iteration even with the most efficient algorithms, which thus cannot scale to large graphs (Friedman et al., 2008; Hsieh et al., 2013; 2014).

As Θ is constrained to be a Laplacian-like matrix, finding the optimizer Θ^* in Equation 3 is equivalent to searching for critical edges from a complete graph, which would involve all possible (i.e., $O(n^2)$) edges. Here we say an edge is critical (noncritical) if including it to the graph will significantly increase (decrease) F in Equation 3. Consequently, we can recover the underlying graph by pruning noncritical edges from the complete graph. Nonetheless, storing a complete graph still requires quadratic complexity. To have a near-linear algorithm for clean graph recovery, instead of searching within the complete graph we limit our search within an initial base graph \mathcal{G}_{base} that is much sparser than the complete graph but dense enough for identifying the candidate edges critical for recovering the clean graph. Subsequently, the final graphical model (graph Laplacian) can be obtained by further pruning noncritical edges from \mathcal{G}_{base} .

3.2. Base Graph Construction

During the first phase of GARNET, as shown in Figure 2, our goal is to build a base graph \mathcal{G}_{base} , which allows greatly reducing the search space caused by a potential complete graph without taking the risk of losing critical candidate edges that are key to clean graph recovery. To this end, we give the following theorem:

Theorem 3.3. *Given a graph $\mathcal{G} = (\mathcal{V}, \mathcal{E})$ and its normalized Laplacian matrix L_G , let V_i denote the weighted spectral embedding of node i by using top r eigenpairs of L_G . Suppose V_i is normalized, i.e., $\|V_i\|_2 = 1$, and a relatively small r is picked such that $\lambda_r \leq 1$, where λ_r is the r -th smallest eigenvalue of L_G , then we have:*

$$\sum_{(i,j) \in \mathcal{E}} \|V_i - V_j\|_2^2 \leq 0.25r \quad (4)$$

Our proof for Theorem 3.3 is available in Appendix B. Note that r is a small constant, which is independent of the graph size. Thus, Theorem 3.3 indicates that, if an edge connects nodes i and j in the clean graph, then the Euclidean distance between the weighted spectral embeddings of these two nodes will be small, which motivates us to build a nearest neighbor (NN) graph as \mathcal{G}_{base} to incorporate those clean edges.

Concretely, we first obtain the weighted spectral embedding matrix V of the input adversarial graph \mathcal{G}_{adv} to represent that of the underlying clean graph \mathcal{G}_{clean} , as V consists of dominant singular components that are shared by \mathcal{G}_{adv} and \mathcal{G}_{clean} (Entezari et al., 2020). We then leverage V to construct an NN graph, where each node is connected to its k most similar nodes based on the Euclidean distance between their spectral embeddings. In this work, we exploit an approximate k-nearest neighbor algorithm for constructing the NN graph, which has $O(|\mathcal{V}| \log |\mathcal{V}|)$ complexity and thus can scale to very large graphs (Malkov & Yashunin, 2018). By choosing a proper k (e.g., $k = 50 \sim 100$), \mathcal{G}_{base} is likely to cover edges in the underlying clean graph. Thus, \mathcal{G}_{base} can serve as a reasonable search space for identifying critical edges in the next step.

3.3. Graph Refinement via Edge Pruning

For the second phase of GARNET shown in Figure 2, we refine \mathcal{G}_{base} by aggressively pruning noncritical edges from \mathcal{G}_{base} , such that the refined graph only preserves the most important edges that contribute most to the log-likelihood F in Equation 3.

To identify critical (noncritical) edges that can most effectively increase (decrease) F , we exploit the update of Θ based on gradient ascent: $\Theta \leftarrow \Theta + \eta \frac{\partial F}{\partial \Theta}$, where η is the step size. As mentioned in Section 2.1, Θ is constrained to be $L + \frac{I}{\sigma^2}$, which means the off-diagonal elements in Θ correspond to negative of edge weights in the underlying

graph, i.e., $\Theta_{i,j} = -w_{i,j}$. Thus, the update of $\Theta_{i,j}$ during gradient ascent can be viewed as:

$$\Theta_{i,j} \leftarrow \Theta_{i,j} + \eta \left(\frac{\partial F}{\partial \Theta} \right)_{i,j} = \Theta_{i,j} - \eta \frac{\partial F}{\partial w_{i,j}} \quad (5)$$

Equation 5 means that, if $\frac{\partial F}{\partial w_{i,j}}$ is large and positive, $\Theta_{i,j}$ will become more negative, which corresponds to increasing the edge weight in the underlying graph. Similarly, if $\frac{\partial F}{\partial w_{i,j}}$ is small and negative, $\Theta_{i,j}$ will be less negative, corresponding to decreasing the edge weight. In other words, the edge weight $w_{i,j}$ with a large (small) $\frac{\partial F}{\partial w_{i,j}}$ should be increased (decreased) to maximize the log-likelihood F , meaning the corresponding edge is critical (noncritical). Thus, we can identify the critical edges once we know $\frac{\partial F}{\partial w_{i,j}}$. By setting $\alpha = 0$ in Equation 3 and taking the partial derivative with respect to an edge weight $w_{i,j}$, we have:

$$\frac{\partial F}{\partial w_{i,j}} = \sum_{k=1}^n \frac{1}{\lambda_k + 1/\sigma^2} \frac{\partial \lambda_k}{\partial w_{i,j}} - \frac{\|V^T e_{i,j}\|_2^2}{r} \quad (6)$$

where $\lambda_k, \forall k = 1, 2, \dots, n$ are the Laplacian eigenvalues of a given graph (e.g., \mathcal{G}_{base}), $e_{i,j} = e_i - e_j$, and e_i denotes the vector with all zero entries except for the i -th entry being 1.

Theorem 3.4 (Feng (2021)). *Let λ_k and u_k be the k -th eigenvalue and the corresponding eigenvector of the Laplacian matrix, respectively. The spectral perturbation $\delta \lambda_k$ due to the increase of an edge weight $w_{i,j}$ can be estimated by:*

$$\delta \lambda_k = \delta w_{i,j} (u_k^T e_{i,j})^2 \quad (7)$$

The proof for Theorem 3.4 is available in Feng (2021). According to Theorem 3.4 and Equation 6, we can estimate $\frac{\partial F}{\partial w_{i,j}}$ in the following:

$$\frac{\partial F}{\partial w_{i,j}} \approx \|U^T e_{i,j}\|_2^2 - \frac{1}{r} \|V^T e_{i,j}\|_2^2 \quad (8)$$

where $U = [\frac{u_1}{\sqrt{\lambda_1 + 1/\sigma^2}}, \dots, \frac{u_r}{\sqrt{\lambda_r + 1/\sigma^2}}]$, λ_i is the i -th smallest Laplacian eigenvalue of \mathcal{G}_{base} , and u_i is the corresponding eigenvector. Consequently, an edge (i, j) is critical if $\|U^T e_{i,j}\|_2^2 \gg \frac{1}{r} \|V^T e_{i,j}\|_2^2$. As V and U are the spectral embeddings on the input adversarial graph and the base graph, respectively, we define the **spectral embedding distortion** $s_{i,j}$ below to measure the edge importance:

$$s_{i,j} = \frac{\|U^T e_{i,j}\|_2^2}{\|V^T e_{i,j}\|_2^2} \quad (9)$$

Based on Equation 9, we prune edges in the base graph \mathcal{G}_{base} that have small spectral embedding distortion, i.e., $s_{i,j} < \gamma$, where γ is a hyperparameter to control the sparsity of the refined graph. Hence, the refined base graph \mathcal{G}'_{base} largely recovers the underlying clean graph structure from the input adversarial graph. Since \mathcal{G}'_{base} is constructed by only leveraging the top few dominant singular components

of \mathcal{G}_{adv} , it ignores the high-rank adversarial components and thus robust to adversarial attacks. As a result, we can vaccinate a given GNN model by training it on \mathcal{G}'_{base} to improve its robustness, which is the last phase of GARNET.

3.4. Complexity of GARNET

The first phase of GARNET requires $O(r|\mathcal{E}|)$ time for computing top r Laplacian eigenpairs (Baglama & Reichel, 2005), and $O(|\mathcal{V}| \log |\mathcal{V}|)$ time for kNN graph construction (Malkov & Yashunin, 2018). The second phase involves $O(rk|\mathcal{V}|)$ time for computing spectral embeddings and edge pruning on the kNN graph. Thus, the overall time complexity for graph purification is $O(r(|\mathcal{E}| + k|\mathcal{V}|) + |\mathcal{V}| \log |\mathcal{V}|)$, where $|\mathcal{V}|$ and $|\mathcal{E}|$ denote the number of nodes and edges in the adversarial graph, respectively, and k is the averaged node degree in the kNN graph. We further provide the space complexity of GARNET in Appendix F.

4. Experiments

We have conducted comparative evaluation of GARNET against state-of-the-art defense GNN models under targeted attack (Nettack) (Zügner et al., 2018) and non-targeted attack (Metattack) (Zügner & Günemann, 2019) with different perturbation budgets, on both homophilic and heterophilic datasets. Besides, we further show the scalability of GARNET by comparing its run time with prior defense methods and evaluating GARNET on ogbn-products, which consists of more than 2 million nodes and 60 million edges (Hu et al., 2020). Due to the space limitation, the ablation studies of GARNET on kNN graph construction and edge pruning are available in Appendix G.

Experimental Setup. The details of datasets used in our experiments are available in Appendix C. We choose as baselines two state-of-the-art defense methods based on graph purification: TSVD (Entezari et al., 2020) and Pro-GNN (Jin et al., 2020). Moreover, we use GCN (Kipf & Welling, 2016) and GPRGNN (Chien et al., 2021) as the backbone GNN models for defense on homophilic datasets (i.e., Cora and Pubmed). As GCN performs poorly on heterophilic datasets (Zhu et al., 2020), we only choose GPRGNN as the backbone model on Chameleon and Squirrel datasets. More details of the backbone models are available in Appendix H. For all baselines, we tune their hyperparameters against adversarial attacks with a small perturbation, and keep the same hyperparameters for larger adversarial perturbations. We further show hyperparameter settings of GARNET and our hardware information in Appendices D and E.

4.1. Defense Against Targeted Attack

We first evaluate the model robustness against Nettack, a strong attack method that can fool a GNN model to mis-

Table 1. Averaged node classification accuracy (%) \pm std under targeted attack (Nettack) with different perturbation ratio — We denote the evaluated dataset by its name with the number of perturbations (e.g., Cora-0 means the clean Cora graph and Cora-1 denotes there is 1 adversarial edge perturbation per target node). As GCN is not designed for heterophilic graphs, we only show results of defense methods with GPRGNN as the backbone model on Chameleon and Squirrel. We bold and underline the first and second highest accuracy of each backbone GNN model, respectively. *OOM* means out of memory.

Dataset	GCN				GPRGNN			
	Vanilla	TSVD	ProGNN	GARNET	Vanilla	TSVD	ProGNN	GARNET
Cora-0	<u>80.96</u> \pm 0.95	72.65 \pm 2.29	80.54 \pm 1.21	81.08 \pm 2.05	83.04 \pm 2.05	81.68 \pm 1.78	82.04 \pm 1.33	<u>82.77</u> \pm 1.89
Cora-1	70.06 \pm 0.81	71.36 \pm 1.63	81.65 \pm 0.59	<u>79.75</u> \pm 2.35	<u>81.68</u> \pm 2.18	79.36 \pm 2.23	80.56 \pm 1.71	82.17 \pm 1.95
Cora-2	68.60 \pm 1.81	70.66 \pm 2.76	79.83 \pm 1.10	<u>79.69</u> \pm 1.50	74.34 \pm 2.41	<u>76.26</u> \pm 2.34	76.12 \pm 2.43	78.55 \pm 2.11
Cora-3	65.04 \pm 3.31	68.20 \pm 1.93	<u>72.08</u> \pm 1.20	74.42 \pm 2.06	70.96 \pm 2.00	70.90 \pm 3.89	<u>73.74</u> \pm 2.73	79.40 \pm 1.35
Cora-4	61.69 \pm 1.48	65.34 \pm 3.46	<u>67.83</u> \pm 1.87	69.60 \pm 2.67	65.90 \pm 1.61	65.51 \pm 3.27	<u>68.94</u> \pm 3.25	72.77 \pm 2.16
Cora-5	55.66 \pm 1.95	60.30 \pm 2.25	<u>65.38</u> \pm 1.65	67.04 \pm 2.05	62.89 \pm 1.95	63.52 \pm 3.27	<u>63.74</u> \pm 2.57	71.45 \pm 2.73
Pubmed-0	<u>87.26</u> \pm 0.51	87.03 \pm 0.48	<i>OOM</i>	87.96 \pm 0.58	<u>90.05</u> \pm 0.73	<i>OOM</i>	<i>OOM</i>	90.99 \pm 0.52
Pubmed-1	84.29 \pm 0.68	<u>86.46</u> \pm 0.28	<i>OOM</i>	87.03 \pm 0.68	<u>89.30</u> \pm 0.54	<i>OOM</i>	<i>OOM</i>	90.91 \pm 0.47
Pubmed-2	82.17 \pm 0.67	<u>83.68</u> \pm 0.46	<i>OOM</i>	86.92 \pm 0.45	<u>87.42</u> \pm 0.28	<i>OOM</i>	<i>OOM</i>	90.75 \pm 0.55
Pubmed-3	81.13 \pm 0.53	<u>81.34</u> \pm 0.68	<i>OOM</i>	86.50 \pm 0.45	<u>84.46</u> \pm 0.53	<i>OOM</i>	<i>OOM</i>	90.70 \pm 0.37
Pubmed-4	75.48 \pm 0.52	<u>82.41</u> \pm 0.54	<i>OOM</i>	86.44 \pm 0.64	<u>81.72</u> \pm 0.72	<i>OOM</i>	<i>OOM</i>	90.11 \pm 0.57
Pubmed-5	66.67 \pm 1.34	<u>79.56</u> \pm 0.48	<i>OOM</i>	86.12 \pm 0.86	<u>76.99</u> \pm 1.16	<i>OOM</i>	<i>OOM</i>	89.52 \pm 0.45
Chameleon-0	/				71.46 \pm 1.92	62.12 \pm 3.04	58.80 \pm 1.72	72.89 \pm 2.65
Chameleon-1					71.02 \pm 1.57	61.34 \pm 2.93	58.05 \pm 1.90	72.68 \pm 1.89
Chameleon-2					<u>70.71</u> \pm 1.12	61.09 \pm 2.80	57.44 \pm 1.67	72.20 \pm 2.31
Chameleon-3					<u>70.30</u> \pm 1.28	60.98 \pm 2.82	57.19 \pm 1.83	72.17 \pm 2.07
Chameleon-4					<u>69.87</u> \pm 1.29	60.85 \pm 3.31	57.44 \pm 1.63	72.06 \pm 2.94
Chameleon-5					<u>66.26</u> \pm 1.71	60.37 \pm 2.86	57.07 \pm 1.82	71.83 \pm 2.11
Squirrel-0	/				41.36 \pm 2.87	32.98 \pm 2.36	31.81 \pm 1.72	44.91 \pm 1.53
Squirrel-1					41.27 \pm 3.16	32.63 \pm 0.87	30.54 \pm 2.45	43.55 \pm 1.79
Squirrel-2					<u>41.09</u> \pm 2.14	32.05 \pm 1.05	30.73 \pm 2.13	44.09 \pm 2.35
Squirrel-3					<u>40.98</u> \pm 2.72	32.00 \pm 1.66	30.25 \pm 1.98	44.18 \pm 2.26
Squirrel-4					<u>40.25</u> \pm 2.82	31.45 \pm 1.38	29.09 \pm 2.33	43.73 \pm 1.62
Squirrel-5					<u>39.45</u> \pm 2.36	31.20 \pm 1.84	27.27 \pm 1.87	43.64 \pm 1.53

classify some target nodes with a few structure (edge) perturbations. We choose the same set of target nodes as in (Jin et al., 2020) and the attack budget varies from 0 to 5 perturbations per target node.

Table 1 reports the average accuracy over 10 runs on two homophilic datasets (i.e., Cora and Pubmed) and two heterophilic datasets (i.e., Chameleon and Squirrel). It shows that GARNET, with either a backbone GNN model (GCN or GPRGNN), outperforms defense baselines in terms of clean accuracy across all datasets. Moreover, GARNET achieves the highest adversarial robustness in most cases, improving the accuracy by up to 9.96% and 12.44% over defense methods on homophilic and heterophilic datasets, respectively. We attribute the significant accuracy improvement to GARNET’s strengths in recovering key structures of the clean graph while ignoring the high-rank adversarial components during graph purification. Notably, the accuracy degradation of GARNET when increasing the perturbation budget is much smaller than that of baselines. For instance, the accuracy drop of GARNET is only 1.39% with perturbations varying from 1 to 5 on Pubmed, while the accuracy of defense baselines drops by at least 6.9%, indicating GARNET is indeed more robust to the strong targeted attack.

Table 1 also shows that the two defense baselines fail to

defend GPRGNN on heterophilic graphs and even degrade the accuracy of the vanilla GPRGNN by a large margin. The reason why ProGNN performs poorly is that it follows the graph homophily assumption for improving GNN robustness, which contradicts the property of heterophilic graphs. For the TSVD-based defense method, the low-rank graph generated by TSVD contains negative edge weights, which degrade the performance of GPRGNN for adapting its graph filter on heterophilic graphs (Chien et al., 2021). In contrast, GARNET purifies the adversarial graph without any assumptions on the homophily property of the underlying graph; it produces a graph with no negative edge weights, leading to much higher accuracies on heterophilic datasets.

4.2. Defense Against Non-Targeted Attack

We further evaluate model robustness against a strong non-targeted attack, i.e., Metattack, whose goal is to drop the overall accuracy of the whole test set with a given perturbation ratio budget (i.e., the number of adversarial edges over the number of total edges). We report the averaged accuracy over 10 runs in Table 2 with perturbation ratio in {0%, 10%, 20%}. As shown in Table 2, GARNET gains up to 2.84% and 13.27% accuracy improvement over the defense baselines on homophilic and heterophilic datasets,

Table 2. Averaged node classification accuracy (%) \pm std under non-targeted attack (Metattack) with different perturbation ratio — We denote the evaluated dataset by its name with the perturbation ratio (e.g., Cora-0 means the clean Cora graph and Cora-10 denotes there are 10% adversarial edges). As GCN is not designed for heterophilic graphs, we only show results of defense methods with GPRGNN as the backbone model on Chameleon and Squirrel. We bold and underline the first and second highest accuracy of each backbone GNN model, respectively. *OOM* means out of memory.

Dataset	GCN				GPRGNN			
	Vanilla	TSVD	ProGNN	GARNET	Vanilla	TSVD	ProGNN	GARNET
Cora-0	81.35 \pm 0.66	73.86 \pm 0.53	78.56 \pm 0.36	<u>79.64</u> \pm 0.75	83.05 \pm 0.42	81.61 \pm 0.54	82.04 \pm 0.90	<u>82.67</u> \pm 1.89
Cora-10	69.50 \pm 1.46	69.45 \pm 0.69	77.90 \pm 0.69	<u>77.78</u> \pm 0.53	80.37 \pm 0.65	<u>81.08</u> \pm 0.52	80.31 \pm 1.23	82.17 \pm 0.69
Cora-20	56.28 \pm 1.19	62.44 \pm 1.16	<u>72.28</u> \pm 1.67	73.89 \pm 0.91	74.27 \pm 2.11	<u>78.50</u> \pm 1.20	76.29 \pm 1.46	81.34 \pm 0.79
Pubmed-0	87.16 \pm 0.09	84.53 \pm 0.08	<i>OOM</i>	<u>85.37</u> \pm 0.20	87.35 \pm 0.13	<i>OOM</i>	<i>OOM</i>	<u>86.86</u> \pm 0.57
Pubmed-10	81.16 \pm 0.13	<u>84.56</u> \pm 0.10	<i>OOM</i>	85.22 \pm 0.13	<u>85.52</u> \pm 0.14	<i>OOM</i>	<i>OOM</i>	86.24 \pm 0.20
Pubmed-20	77.20 \pm 0.27	<u>84.30</u> \pm 0.08	<i>OOM</i>	85.14 \pm 0.23	<u>84.18</u> \pm 0.15	<i>OOM</i>	<i>OOM</i>	85.69 \pm 0.26
Chameleon-0					61.36 \pm 1.00	47.29 \pm 1.63	48.39 \pm 0.68	<u>61.11</u> \pm 2.46
Chameleon-10					<u>57.55</u> \pm 1.26	47.07 \pm 1.21	47.80 \pm 0.91	60.96 \pm 1.22
Chameleon-20					<u>53.20</u> \pm 0.88	45.12 \pm 1.34	46.69 \pm 0.61	59.96 \pm 0.84
Squirrel-0					<u>39.51</u> \pm 1.64	31.36 \pm 1.87	31.64 \pm 2.87	43.43 \pm 1.14
Squirrel-10					<u>38.27</u> \pm 0.83	28.25 \pm 1.66	30.33 \pm 3.29	42.62 \pm 1.09
Squirrel-20					<u>35.22</u> \pm 1.20	23.91 \pm 1.40	29.36 \pm 3.61	41.97 \pm 1.02

respectively, which further confirms that GARNET is resistant to adversarial attacks. It is worth noting that TSVD and ProGNN involve dense matrices during GNN training. Both methods run out of GPU memory even on Pubmed, whose graph only contains 20k nodes. In contrast, GARNET is not only robust to adversarial attacks, but also scalable to large graphs, as empirically shown in Section 4.3.

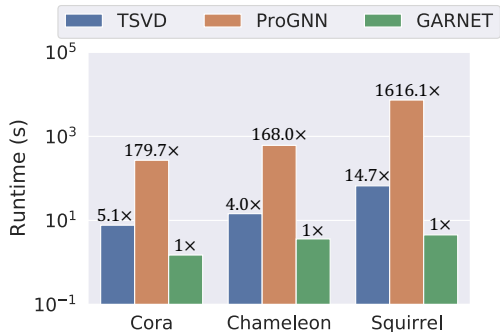


Figure 3. End-to-end runtime comparison of GARNET and prior defense methods. We use GPRGNN as the backbone GNN model.

Table 3. Averaged clean and adversarial accuracy (%) \pm std under non-targeted attack (DICE) with 70% perturbation ratio.

Method	ogbn-arxiv-DICE		ogbn-products-DICE	
	Clean	Adversarial	Clean	Adversarial
GPRGNN	68.04 \pm 0.23	56.28 \pm 0.37	72.64 \pm 0.09	64.33 \pm 0.12
GARNET	67.15 \pm 0.42	62.69 \pm 0.22	71.35 \pm 0.11	70.38 \pm 0.17

4.3. Scalability of GARNET

To demonstrate the scalability of GARNET, we first compare the run time of GARNET with prior low-rank defense methods. As shown in Figure 3, the TSVD defense method

is slower than GARNET since it produces a dense adjacency matrix that slows down the GNN training. Moreover, ProGNN is extremely slow as it jointly learns the low-rank graph structure and the robust GNN model, which requires performing TSVD for every epoch. In contrast, GARNET can efficiently produce a sparse graph for downstream GNN training, leading to end-to-end runtime speedup over prior methods by up to 14.7 \times . In addition, we further evaluate the robustness of GARNET with GPRGNN as the backbone model on two large datasets: ogbn-arxiv and ogbn-products. Given that existing strongest attacks (Nettack and Metattack) are not scalable to large graphs, we leverage a less powerful yet more scalable attacking algorithm called DICE (Wanick et al., 2018), which randomly connects (disconnects) nodes from different (same) classes, to perturb the graph structure. To have a challenging defense scenario, we consider a 70% perturbation ratio for DICE. Note that both TSVD and ProGNN run out of memory on these two datasets. Table 3 shows that GARNET-GPRGNN slightly degrades the clean accuracy but improves the adversarial accuracy over vanilla GPRGNN by a margin of 6.41% and 6.05% on ogbn-arxiv and ogbn-products, respectively. This means GARNET can also defend GNN models on large datasets.

5. Conclusions

This work introduces GARNET, a spectral approach to robust and scalable graph neural networks by combining spectral embedding and the probabilistic graphical model. GARNET first uses weighted spectral embedding to construct a base graph, which is then refined by pruning uncritical edges based on the graphical model. Results show that GARNET not only outperforms state-of-the-art defense models, but also scales to large graphs with millions of nodes.

References

- Akiba, T., Sano, S., Yanase, T., Ohta, T., and Koyama, M. Optuna: A next-generation hyperparameter optimization framework. In *Proceedings of the 25th ACM SIGKDD international conference on knowledge discovery & data mining*, pp. 2623–2631, 2019.
- Baglama, J. and Reichel, L. Augmented implicitly restarted lanczos bidiagonalization methods. *SIAM Journal on Scientific Computing*, 27(1):19–42, 2005.
- Banerjee, O., El Ghaoui, L., and d’Aspremont, A. Model selection through sparse maximum likelihood estimation for multivariate gaussian or binary data. *The Journal of Machine Learning Research*, 9:485–516, 2008.
- Casas, S., Gulino, C., Liao, R., and Urtasun, R. Spaggn: Spatially-aware graph neural networks for relational behavior forecasting from sensor data. In *2020 IEEE International Conference on Robotics and Automation (ICRA)*, pp. 9491–9497. IEEE, 2020.
- Chien, E., Peng, J., Li, P., and Milenkovic, O. Adaptive universal generalized pagerank graph neural network. In *International Conference on Learning Representations*, 2021. URL <https://openreview.net/forum?id=n6jl7fLxrP>.
- Dai, H., Li, H., Tian, T., Huang, X., Wang, L., Zhu, J., and Song, L. Adversarial attack on graph structured data. In *International conference on machine learning*, pp. 1115–1124. PMLR, 2018.
- Dong, X., Thanou, D., Frossard, P., and Vandergheynst, P. Learning laplacian matrix in smooth graph signal representations. *IEEE Transactions on Signal Processing*, 64(23):6160–6173, 2016.
- Dong, X., Thanou, D., Rabbat, M., and Frossard, P. Learning graphs from data: A signal representation perspective. *IEEE Signal Processing Magazine*, 36(3):44–63, 2019.
- Egilmez, H. E., Pavez, E., and Ortega, A. Graph learning from data under laplacian and structural constraints. *IEEE Journal of Selected Topics in Signal Processing*, 11(6): 825–841, 2017.
- Entezari, N., Al-Sayouri, S. A., Darvishzadeh, A., and Papalexakis, E. E. All you need is low (rank) defending against adversarial attacks on graphs. In *Proceedings of the 13th International Conference on Web Search and Data Mining*, pp. 169–177, 2020.
- Feng, Z. Sgl: Spectral graph learning from measurements. *arXiv preprint arXiv:2104.07867*, 2021.
- Friedman, J., Hastie, T., and Tibshirani, R. Sparse inverse covariance estimation with the graphical lasso. *Biostatistics*, 9(3):432–441, 2008.
- Golub, G. H. and Van Loan, C. F. *Matrix computations*, volume 3. JHU press, 2013.
- Hamilton, W. L. Graph representation learning. *Synthesis Lectures on Artificial Intelligence and Machine Learning*, 14(3):1–159, 2020.
- Hsieh, C.-J., Sustik, M. A., Dhillon, I. S., and Ravikumar, P. Sparse inverse covariance matrix estimation using quadratic approximation. *arXiv preprint arXiv:1306.3212*, 2013.
- Hsieh, C.-J., Sustik, M. A., Dhillon, I. S., Ravikumar, P., et al. Quic: quadratic approximation for sparse inverse covariance estimation. *J. Mach. Learn. Res.*, 15(1):2911–2947, 2014.
- Hu, W., Fey, M., Zitnik, M., Dong, Y., Ren, H., Liu, B., Catasta, M., and Leskovec, J. Open graph benchmark: Datasets for machine learning on graphs. *arXiv preprint arXiv:2005.00687*, 2020.
- Huang, Q., He, H., Singh, A., Lim, S.-N., and Benson, A. R. Combining label propagation and simple models out-performs graph neural networks. *arXiv preprint arXiv:2010.13993*, 2020.
- Jin, W., Ma, Y., Liu, X., Tang, X., Wang, S., and Tang, J. Graph structure learning for robust graph neural networks. In *Proceedings of the 26th ACM SIGKDD International Conference on Knowledge Discovery & Data Mining*, pp. 66–74, 2020.
- Kalofolias, V. and Perraudin, N. Large scale graph learning from smooth signals. *International Conference on Learning Representations (ICLR 2019)*, 2019.
- Kipf, T. N. and Welling, M. Semi-supervised classification with graph convolutional networks. *arXiv preprint arXiv:1609.02907*, 2016.
- Li, Y., Jin, W., Xu, H., and Tang, J. Deeprobust: A pytorch library for adversarial attacks and defenses. *arXiv preprint arXiv:2005.06149*, 2020.
- Malkov, Y. A. and Yashunin, D. A. Efficient and robust approximate nearest neighbor search using hierarchical navigable small world graphs. *IEEE transactions on pattern analysis and machine intelligence*, 42(4):824–836, 2018.
- Mirhoseini, A., Goldie, A., Yazgan, M., Jiang, J. W., Songhori, E., Wang, S., Lee, Y.-J., Johnson, E., Pathak, O., Nazi, A., et al. A graph placement methodology for fast chip design. *Nature*, 594(7862):207–212, 2021.

-
- Rozemberczki, B., Allen, C., and Sarkar, R. Multi-scale attributed node embedding. *Journal of Complex Networks*, 9(2):cnab014, 2021.
- Senior, A. W., Evans, R., Jumper, J., Kirkpatrick, J., Sifre, L., Green, T., Qin, C., Žídek, A., Nelson, A. W., Bridgland, A., et al. Improved protein structure prediction using potentials from deep learning. *Nature*, 577(7792): 706–710, 2020.
- Slawski, M. and Hein, M. Estimation of positive definite m-matrices and structure learning for attractive gaussian markov random fields. *Linear Algebra and its Applications*, 473:145–179, 2015.
- Sun, L., Dou, Y., Yang, C., Wang, J., Yu, P. S., He, L., and Li, B. Adversarial attack and defense on graph data: A survey. *arXiv preprint arXiv:1812.10528*, 2018.
- Waniek, M., Michalak, T. P., Wooldridge, M. J., and Rahman, T. Hiding individuals and communities in a social network. *Nature Human Behaviour*, 2(2):139–147, 2018.
- Yang, Z., Cohen, W., and Salakhudinov, R. Revisiting semi-supervised learning with graph embeddings. In *International conference on machine learning*, pp. 40–48. PMLR, 2016.
- Ying, R., He, R., Chen, K., Eksombatchai, P., Hamilton, W. L., and Leskovec, J. Graph convolutional neural networks for web-scale recommender systems. In *Proceedings of the 24th ACM SIGKDD International Conference on Knowledge Discovery & Data Mining*, pp. 974–983, 2018.
- Zhu, J., Yan, Y., Zhao, L., Heimann, M., Akoglu, L., and Koutra, D. Beyond homophily in graph neural networks: Current limitations and effective designs. *arXiv preprint arXiv:2006.11468*, 2020.
- Zhu, J., Jin, J., Schaub, M. T., and Koutra, D. Improving robustness of graph neural networks with heterophily-inspired designs. *arXiv preprint arXiv:2106.07767*, 2021.
- Zügner, D. and Günnemann, S. Adversarial attacks on graph neural networks via meta learning. *arXiv preprint arXiv:1902.08412*, 2019.
- Zügner, D., Akbarnejad, A., and Günnemann, S. Adversarial attacks on neural networks for graph data. In *Proceedings of the 24th ACM SIGKDD International Conference on Knowledge Discovery & Data Mining*, pp. 2847–2856, 2018.

A. Proof for Theorem 3.2

Proof. As the graph is undirected, we can perform eigendecomposition on both A_{norm} and L_{norm} to obtain their real eigenvalues and the corresponding eigenvectors. Let λ_i , $\hat{\lambda}_i$, and σ_i , $i = 1, 2, \dots, r$ denote the r smallest eigenvalues of L_{norm} , r largest eigenvalues of A_{norm} , and r largest singular values of A_{norm} , respectively. Since $A_{norm} = I - L_{norm}$, A_{norm} and L_{norm} share the same set of eigenvectors while their eigenvalues satisfy: $\hat{\lambda}_i = 1 - \lambda_i$, $i = 1, 2, \dots, r$. Moreover, since we assume that the r largest magnitude eigenvalues of A_{norm} are non-negative, we have $\sigma_i = |\hat{\lambda}_i| = \hat{\lambda}_i$, $i = 1, 2, \dots, r$. Thus, we have:

$$\begin{aligned}
VV^T &= [v_1, \dots, v_r] \begin{bmatrix} |1 - \lambda_1| & & \\ & \ddots & \\ & & |1 - \lambda_r| \end{bmatrix} [v_1, \dots, v_r]^T \\
&= [v_1, \dots, v_r] \begin{bmatrix} |\hat{\lambda}_1| & & \\ & \ddots & \\ & & |\hat{\lambda}_r| \end{bmatrix} [v_1, \dots, v_r]^T \\
&= [v_1, \dots, v_r] \begin{bmatrix} \sigma_1 & & \\ & \ddots & \\ & & \sigma_r \end{bmatrix} [v_1, \dots, v_r]^T \\
&= \hat{A}
\end{aligned}$$

□

B. Proof for Theorem 3.3

Proof. Since the weighted embedding matrix V is defined as $V \stackrel{\text{def}}{=} [\sqrt{|1 - \lambda_1|}v_1, \dots, \sqrt{|1 - \lambda_r|}v_r]$, where $\lambda_1, \lambda_2, \dots, \lambda_r$ and v_1, v_2, \dots, v_r are the top r smallest eigenvalues and the corresponding eigenvectors of normalized graph Laplacian matrix $L_{norm} = I - D^{-\frac{1}{2}}AD^{-\frac{1}{2}}$, we have:

$$\begin{aligned}
\sum_{(i,j) \in \mathcal{E}} \|V_i - V_j\|_2^2 &= \sum_{k=1}^r \sum_{(i,j) \in \mathcal{E}} |1 - \lambda_k| (v_{k,i} - v_{k,j})^2 \\
&= \sum_{k=1}^r |1 - \lambda_k| \sum_{(i,j) \in \mathcal{E}} (v_{k,i} - v_{k,j})^2 \\
&= \sum_{k=1}^r |1 - \lambda_k| v_k^T L_{norm} v_k \\
&= \sum_{k=1}^r (1 - \lambda_k) \lambda_k \\
&\leq \sum_{k=1}^r 0.25 \\
&= 0.25r
\end{aligned}$$

□

The fourth equation above is based on Courant-Fischer Theorem (Golub & Van Loan, 2013) with the assumption that $\lambda_r \leq 1$ and $\|v_k\|_2 = 1, \forall k = 1, \dots, r$. The inequality is derived by arithmetic mean-geometric mean (AM-GM) inequality.

Table 4. Statistics of datasets used in our experiments.

Dataset	Type	Homophily Score	Nodes	Edges	Classes	Features
Cora	Homophily	0.80	2,485	5,069	7	1,433
Pubmed	Homophily	0.80	19,717	44,324	3	500
Chameleon	Heterophily	0.23	2,277	62,792	5	2,325
Squirrel	Heterophily	0.22	5,201	396,846	5	2,089
ogbn-arxiv	Homophily	0.66	169,343	1,166,243	40	128
ogbn-products	Homophily	0.81	2,449,029	61,859,140	47	100

C. Dataset Details

Table 4 shows the statistics of the datasets used in our experiments. We follow [Zhu et al. \(2020\)](#) to compute the homophily score per dataset (lower score means more heterophilic). As in [Jin et al. \(2020\)](#), we extract the largest connected components of the original Cora and Pubmed datasets ([Yang et al., 2016](#)) for the adversarial evaluation, with the same train/validation/test split. For Chameleon and Squirrel ([Rozenberczki et al., 2021](#)), we keep the same split setting as [Chien et al. \(2021\)](#). Finally, we follow the split setting of Open Graph Benchmark (OGB) ([Hu et al., 2020](#)) on ogbn-arxiv and ogbn-products.

In addition, we follow [Jin et al. \(2020\)](#) for the selection of target nodes on Cora Pubmed under Nettack. For the Chameleon and Squirrel datasets under Nettack, we choose target nodes that have degrees within the range of $[20, 50]$ and $[20, 140]$, respectively. In regard to non-targeted attacks (i.e., Metattack), we choose nodes in the test set as target nodes for all datasets. We implement all the adversarial attacks based on DeepRobust library ([Li et al., 2020](#)).

D. Hyperparameters Settings of GARNET

Table 5. Summary of hyperparameters in GARNET— We denote the number of eigenpairs for spectral embedding, the number of nearest neighbors for base graph construction, the threshold for edge pruning by r , and the prior data variance k , δ and σ^2 , respectively.

Dataset	r	k	γ	σ^2
Cora-Nettack	50	50	0.05	1000
Cora-Metattack	50	50	0.05	1000
Citeseer-Nettack	50	30	0.003	1000
Citeseer-Metattack	50	60	0.05	1000
Pubmed-Nettack	50	80	0.05	1000
Pubmed-Metattack	50	80	0.05	1000
Chameleon-Nettack	50	60	0.003	1000
Chameleon-Metattack	50	60	0.003	1000
Squirrel-Nettack	50	50	0.003	1000
Squirrel-Metattack	50	50	0.003	1000
ogbn-arxiv-DICE	200	50	0.00003	1000
ogbn-products-DICE	200	50	0.00003	1000

We show the hyperparameters of the reduced-rank approximation kernel and the adaptive filter learning kernel on different datasets under Nettack (1 perturbation per node), Metattack (10% perturbation ratio), and DICE (60% perturbation ratio) in Table 5. For the adaptive label propagation kernel, we do not manually tune hyperparameters but instead leverage Optuna ([Akiba et al., 2019](#)) to optimize the hyperparameters such as the scale β for error correction based on the validation set, since this kernel is fast to compute. We run all GNN training with full batch.

E. Hardware Information

We conduct all experiments on a Linux machine with an Intel Xeon Gold 5218 CPU (8 cores @ 2.30GHz) CPU and 8 NVIDIA RTX 2080 Ti GPU (11 GB memory per GPU).

F. Space Complexity of GARNET

GARNET involves forming a sparse kNN graph by building hierarchical navigable small world (HNSW) graphs (Malkov & Yashunin, 2018) that contain $O(|V| \log |V|)$ nodes in total and each node connects to a fixed number of neighbors. Thus, the space complexity of storing the HNSW graphs is $O(|V| \log |V|)$. In addition, GARNET also needs to store the input adversarial graph and the produced kNN graph. As a result, the total space complexity of GARNET is $O(|V| (\log |V| + k) + |\mathcal{E}|)$, where $|\mathcal{V}|$ and $|\mathcal{E}|$ denote the number of nodes and edges in the adversarial graph, respectively, and k is the averaged node degree in the kNN graph.

Apart from the complexity analysis, we further provide the algorithms of GARNET and TSVD below for comparison.

Algorithm 1 GARNET based adversarial defense (this work)

Input: Adversarial graph \mathcal{G}_{adv} ; node feature matrix $X \in R^{n \times d}$; prior data variance σ^2 ; truncated svd rank r ; kNN graph k ; threshold for edge pruning γ ; a GNN model for defense

Output: Node embedding matrix $Z \in R^{n \times c}$

$M, S = \text{eigs}(\mathcal{G}_{adv}, r)$;

$V = M \sqrt{|I - S|}$;

$\mathcal{G}_{base} = \text{kNN_graph}(V, k)$;

$M', S' = \text{eigs}(\mathcal{G}_{base}, r)$;

$U = M' / \sqrt{S' + I/\sigma^2}$;

for edge $e_{i,j}$ **in** \mathcal{G}_{base} **do**

if $\frac{\|U_i - U_j\|_2^2}{\|V_i - V_j\|_2^2} < \gamma$ **then**

 Prune $e_{i,j}$ from \mathcal{G}_{base} ;

end if

end for

$Z = \text{GNN}(\mathcal{G}'_{base}, X)$;

Algorithm 2 Truncated SVD based adversarial defense (prior work)

Input: Adversarial graph \mathcal{G}_{adv} ; node feature matrix $X \in R^{n \times d}$; truncated svd rank r ; a GNN model for defense

Output: Node embedding matrix $Z \in R^{n \times c}$

$U, S, V = \text{TSVD}(\mathcal{G}_{adv}, r)$;

$A_{\mathcal{G}_{tsvd}} = USV^T$;

$Z = \text{GNN}(\mathcal{G}_{tsvd}, X)$;

G. Ablation Study

G.1. Choice of k for kNN Graph Construction

To evaluate the sensitivity of GARNET to k nearest-neighbor (kNN) graph construction, we evaluate the adversarial accuracy of GARNET with different k values for constructing kNN graphs. Figure 4 shows that the accuracy of GARNET does not change too much when varying k value within the range of $[10, 100]$, indicating a relatively large k (e.g., $k \geq 10$) can enable the kNN graph to incorporate most of edges in the underlying clean graph. Consequently, the performance of GARNET is relatively robust to the choice of k for kNN graph construction. As the peak performance is typically achieved in $[50, 100]$, we recommend choosing $k = 50 \sim 100$ for building the kNN graph in practice.

G.2. Choice of γ for edge pruning

Apart from the choice of k for kNN graph construction, another critical hyperparameter of GARNET is the threshold γ that determines whether an edge should be pruned in the base graph. Thus, we further evaluate the effect of γ on the performance of GARNET. Specifically, we pick γ in the set of $\{0.001, 0.005, 0.01, 0.05, 0.1\}$ and evaluate the corresponding adversarial accuracy of GARNET under Nettack with 1 perturbation per target node. As shown in Figure 5, the improper choice of γ may degrade the adversarial accuracy of GARNET by 3%. However, picking γ around 0.01 can always achieve a reasonable adversarial accuracy on different datasets with different backbone GNN models. As a result, we recommend choosing γ

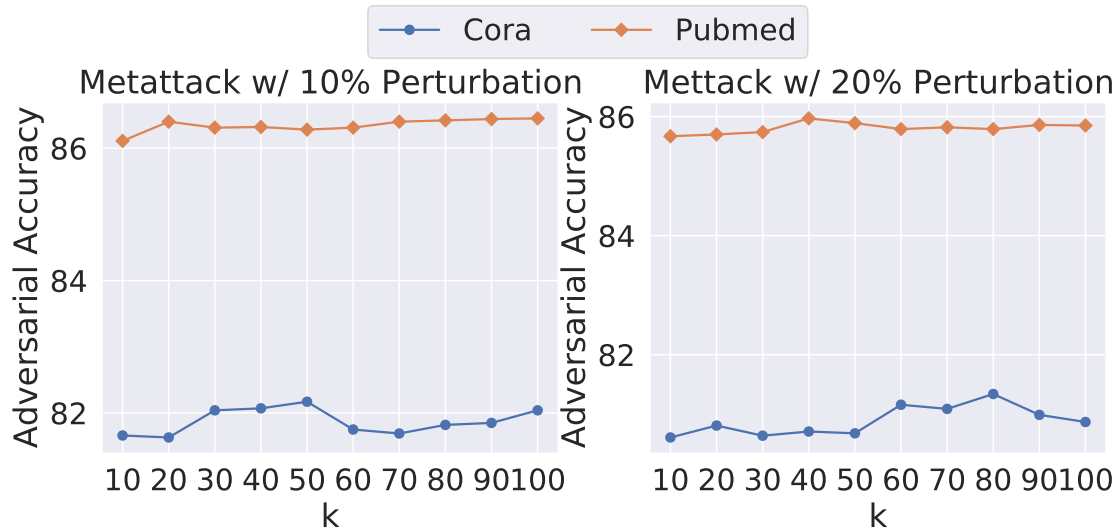


Figure 4. Ablation study of GARNET on k for kNN graph construction.

in the range of $[0.005, 0.05]$ in practice. In addition, Figure 5 also shows that GPRGNN-GARNET is more robust to the changes of γ than GCN-GARNET, which is due to the reason that the adaptive graph filter in GPRGNN can adapt to the graph structure after edge pruning.

H. Backbone GNN Models for Defense

As GARNET can be integrated with any existing GNN models to improve their adversarial accuracy, we choose two popular GNN models as the backbone model in our experiments: GCN (Kipf & Welling, 2016) and GPRGNN (Chien et al., 2021). As GCN model implicitly assume the underlying graph is homophilic, it performs poorly on heterophilic graphs (e.g., Chameleon and Squirrel) (Zhu et al., 2020). In contrast, GPRGNN can work on both homophilic and heterophilic datasets, due to its learned graph filter that can adapt to the homophily/heterophily property of the underlying graph. Thus, we only choose GPRGNN as the backbone model for evaluation on heterophilic datasets. In addition, we add C&S (Huang et al., 2020) to GPRGNN on homophilic graphs (i.e., Cora and Pubmed) for all the defense baselines as well as GARNET.

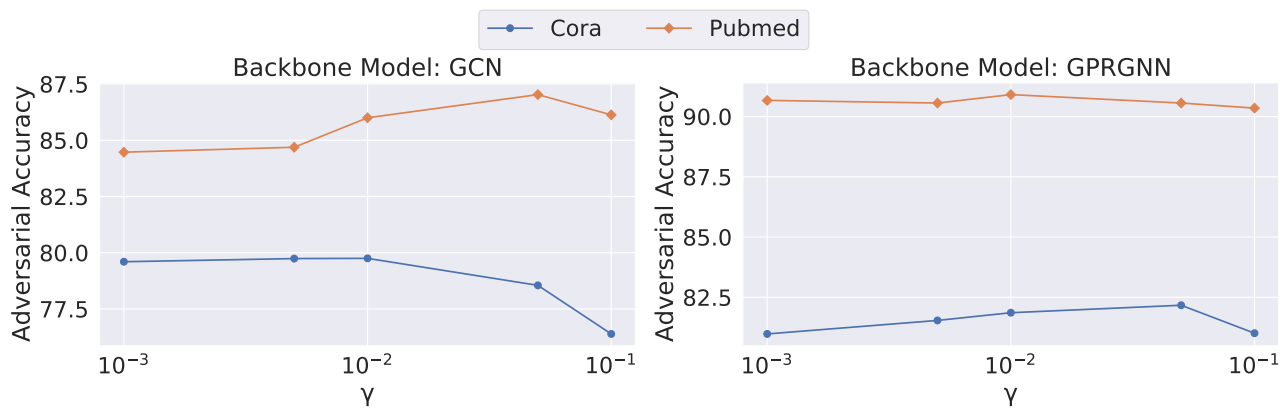


Figure 5. Ablation study of GARNET on threshold γ for edge pruning.